Open-cell foams of polyethylene terephthalate/bisphenol a polycarbonate blend

AUTHOR(S):

Gong, Pengjian; Ohshima, Masahiro

Open-cell Foams of Polyethylene Terephthalate/Bisphenol A Polycarbonate Blend

Authors: Pengjian Gong and Masahiro Ohshima

Affiliation: Department of Chemical Engineering, Kyoto University

Open-cell Foams of Polyethylene Terephthalate/Bisphenol A Polycarbonate Blend

Pengjian Gong and Masahiro Ohshima

Department of Chemical Engineering, Kyoto University, Kyoto 615-8510, Japan

Correspondence to: M. Ohshima (E-mail: ohshima.masahiro.2w@kyoto-u.ac.jp)

ABSTRACT

Open microcellular foams of polyethylene terephthalate (PET)/polycarbonate (PC) blends were prepared by controlling their foaming behavior at the interface between these two polymers. Interface modification was a crucial factor in governing the foaming behavior and cell morphology of the blend foams: annealing at 280°C, i.e., conducting the transesterification reaction, generates a PET-b-PC copolymer, which lowers the interfacial tension, increases the affinity between PET and PC, and decreases the crystallinity of the PET domains. When CO_2 foaming was performed at the interface modified with the copolymer, an interesting fibril-like structure was formed. The cell density of the PET/PC blend then increased, and its cell size reduced to the microscale while maintaining a high open-cell ratio. The effect of heat annealing (transesterification reaction) on CO_2-foaming was studied to reveal the relationship among the interface affinity, crystallinity, and degree of fibrillation. The optimal heat-annealing procedure generated a fibril-like structure in the PET/PC blend foams with a high cell density (7×10^{11} # cm^{-3}), small cell size (less than 2 μm), and 100% open-cell ratio.

KEYWORDS annealing; blends; copolymers; open-cell foam; fibril-like structure;

INTRODUCTION

Polymeric foams have versatile thermal and mechanical properties, and they can be applied to many plastic parts. The application depends on the cell morphology of the foams, which is characterized by the cell density, cell size, and open and/or closed-cell structures. [1] The polymeric foams used for construction, packaging, and heat insulation are commonly made of closed-cell foams. [2] The foams used for shock absorption, sound attenuation, battery separators, and cell-scaffolds for tissue engineering are normally made of open-cell foams. [3-5]

Several cell-opening strategies have been proposed in the field of physical foaming, such as creating high temperature differences between the surface and core of an extrudate, using mixed blowing agents to induce secondary nucleation and to change the cell densities, using interpolymer blending, and blending two polymers with different crystallization temperatures. [6-10] Lee et al. prepared open-cell foams from polyethylene (PE) and polypropylene (PP) blends by extrusion. [9] They proposed two strategies to open the cell wall of the thermoplastic polymer foams: i) The polymer blends were prepared so that their dispersed domains could be composed of a low-T_c (soft) polymer and the matrix could be composed of a high-T_c (hard) polymer. Cell opening was then initiated through the soft domains trapped between growing adjacent cells. ii) The polymer blends were prepared so that their dispersed domains could be composed of a high-T_c (hard) polymer and the matrix could be composed of a low-T_c (soft) polymer. Cell opening was then initiated by debonding the interface between the hard domains and the soft matrix. Lee et al. incorporated a secondary blowing agent to

further plasticize the soft regions so that the stiffness contrast between the hard and soft regions in the polymer blend could be intensified. [7] Kohlhoff et al. used an interpenetrating network structure to increase the stiffness contrast between the domain and matrix and prepared open cellular polylactic acid (PLA)-based blends, in which the monomer acted as another cell-opening agent. [8] To prepare open cellular homopolymer foams, the hard/soft inhomogeneity strategy could be extended to a crystalline/amorphous structure. Semi-crystalline polymers, such as PP, have a hard region in the crystallite and a soft region in the amorphous area. Miyamoto et al. used a crystalline nucleating agent for PP to form three-dimensional network of highly connected nano-fibrils by foaming. [11] The network maintained the cellular size at the nano/microscale level and opened the cell walls by debonding the lamellae from the inter-lamellar amorphous region. Another cell-opening method was reported by Krause et al. [12] They prepared an open cellular polysulfone (PSU) film using CO_2 and tetrahydrofuran (THF) as a blowing agent. During foaming, the cell wall thickness fluctuated, and the degree of fluctuation was facilitated by THF. Consequently, the cell walls were open, and the foam featured nanopores. The authors extended their study to obtain open nanoporous polymers and polymeric blends by CO_2 foaming. [13, 14] Their open nanoporous morphology on the cell wall seemed to be a function of cell wall stretching and certain inhomogeneities in the structural or physical properties. However, the relationship was not clarified, and the mechanism of transition from closed to open cells remained uncertain.

Cell sizes have also been reduced in the foaming industry for the production of microcellular foams. The prevention of cell coalescence was one of the key factors in

reducing the cell size. Cell coalescence and cell size in physical foaming are commonly reduced by increasing the viscosity of the matrix polymer and enhancing the strain hardening behavior. Li et al. numerically simulated polymer foaming to study the dynamics and stability of bubble growth. [15] They found that the stability of bubbles was controlled by the strain hardening characteristics and elastic properties of the polymers. Cross-linking agents and highly viscous components have been used and proven effective to increase the viscoelasticity and suppress cell coalescence. [16, 17] Carbon nanotube, nanoclay, and long-chain branched polymers could also be used to control the viscoelasticity and reduce the cell size. [18-20] They can orient the polymer chains in biaxial elongational flow and increase viscoelasticity locally at the cell wall. To produce open porous microcellular foam, the cell size is reduced while simultaneously opening or rupturing the cell wall. The increase in viscoelasticity and introduction of strain hardening behavior or local polymer orientation can reduce the cell size but might not enhance cell opening. A different strategy is necessary to reduce the cell size, increase the cell density and simultaneously enhance the degree of cell opening.

In this study, the heterogeneous interface was focused on as the site for cell opening. Instead of making the clear contrast between soft and hard domains in the polymer blends, the interfacial properties between the two domains were obscured for cell opening and microcellular foaming. The effect of the interfacial properties on the foaming behavior has been widely investigated. [21-24] Decreasing the interfacial tension between the domain and matrix polymers can increase the compatibility between two polymers and increase the interfacial area, which increases the number of heterogeneous nucleation sites. Conversely, decreasing the interfacial tension reduces the

heterogeneity between the domain and matrix polymers and suppresses the bubble nucleation rate at the interface. [25] Therefore, decreasing the interfacial tension provides positive and negative effects on bubble nucleation. Furthermore, decreasing the interfacial tension can increase the interfacial affinity and lead to a fibril structure that connects the semi-crystalline domains and matrix polymers. [26] Consequently, an optimal interfacial property may exist for microcellular foam with a high open-cell ratio.

Interface modification is a common method for controlling the interfacial tension and blend morphology. In this study, polyethylene terephthalate (PET)/polycarbonate (PC) blends were used to prepare the open porous microcellular foam. In our system, PET dispersed domains were used as bubble nucleating agents. The miscibility between PET and PC was changed by a copolymer produced during the transesterification reaction. [27, 28] The presence of a copolymer at the interface can locally reduce the polymer viscoelasticity at the interface, facilitate stretching, and open the cell wall around the PET domains with a fibrillated structure. The fibrillation at the interface may also lead to a stretch-induced void formation mechanism, which increases the cell density. Therefore, a novel method was reported in this study to control CO_2 foaming with optimal interfacial properties to achieve a designated foam morphology, such as small cell size, large cell density, and large open-cell ratio.

EXPERIMENTAL

Materials

PC (Idemitsu, Taflon A2600, M_w=32,000, MFR=6 g 10-min^{-1} (300°C 1.2 kg)) and PET (Mitsui Chemical, J125, M_w=56,000, inherent viscosity=0.75 dl g^{-1}) were used

as received. CO_2 (99.95% purity, Showa-Tansan, Japan) was used as the physical foaming agent.

Preparation of PET/PC blends

PET and PC pellets were dried in a vacuum oven at room temperature for at least 2 days. They were dry-mixed at two different weight ratios of PET to PC (10/90 and 30/70) and fed into a melt mixer (Labo Plastomill, 4C150 Toyoseiki, Japan). After melt blending, the PET/PC blend was placed in a vacuum oven for another 2 days to remove moisture. The blend was then annealed in an oven at 280°C for two different time periods (1 and 5 h) with a nitrogen purge (heat-annealing process). The transesterification degree was controlled by changing the heat-annealing time. The transesterification reaction can be accelerated by a variety of catalysts, such as lanthanides, titanium and calcium/antimony. [29-31] However, the residual catalysis in PET could carry out the reaction in this study. Therefore, no external catalyst was introduced into our system. Because the PET domain could aggregate when PET/PC 30/70 wt% blends were heat-annealed, the blends were again melt-mixed to increase the dispersion of the PET domains in PC. The sample ID., heat-annealing times, and weight ratios of PET/PC blends are summarized in Table 1.

The first melt-mixing was conducted at 270°C by rotating a kneading rotor at 10 rpm for the first 2 min. The rotation speed was then increased to 50 rpm for the next 8 min. The second melt-mixing was conducted at 10 rpm for 2 min, followed by 50 rpm for 3 min. After mixing, the blends were molded into a plate shape using a hot compression molding machine.

CO_2 foaming

The PET/PC blend samples were placed in a high-pressure autoclave to dissolve the CO_2 at 10 MPa for 22.3 h at 60°C. After removing the sample from the autoclave without foaming, it was immediately placed on an aluminum plate and foamed on the hot press by heating for 1 min at three different foaming temperatures: 80, 120 and 150°C. The sorption time was fixed at 22.3 h to ensure that all blends reached an equilibrium state with CO_2.

Characterization of PET/PC blend rheological properties and crystallinity

The rheological properties were measured using a rheometer (Advanced Rheometric Expansion System, ARES, TA Instruments, USA): Rectangular torsion geometry was used to conduct dynamic temperature ramp tests from 40 to 200°C at a heating rate of 2°C min^{-1}. The constant oscillation frequency of the torsion bar was set to 1 rad s^{-1} with 0.1% constant strain. G'' was measured and used to identify the glass transition temperature (T_g) of neat PET (T_{gPET}), neat PC (T_{gPC}), and the PET domain ($T_g^{'}$) and PC matrix ($T_g^{''}$) in blends. Rectangular torsion geometry was also used for the dynamic frequency sweep tests at temperatures below 200°C in the frequency range of 0.01-100 rad s^{-1}. The strain was set in the range of 0.1-0.4%. When the measurement temperature was higher than 200°C, the parallel plate geometry was used for the dynamic frequency sweep tests at strains of 5-15%. Prior to the dynamic frequency sweep tests, a strain sweep test was conducted to determine the strain limit for a linear viscoelastic response. A master curve of the G'-frequency was then obtained at 150°C. To calculate the interfacial tension, the blends were first placed between two parallel plates at 260°C for 5 min to completely melt the crystals in the PET domains. The blends then underwent dynamic frequency sweep tests at 250°C. The blends were confirmed to remain

amorphous during the tests. The extensional viscosity (uniaxial extensional viscosity) was measured with a fixture. Four strain rates, 0.1, 0.2, 0.5, and 1.0 s^{-1}, were applied to PC, A0, and A1 at 240°C. The testing temperature for sample A5 was set to 220°C to prevent the sample from sagging during the measurement. The samples for the rectangular torsion test were approximately 10 mm in width, 1 mm in thickness, and 40 mm in length. The samples for the parallel plate test were 25 mm in diameter and 2 mm in thickness. The geometry for the samples for the uniaxial elongational viscosity measurement was 18 mm × 10 mm × 0.7 mm. A differential scanning calorimeter (DSC: Pyris 1 Perkin Elmer) was used to measure the crystallinity of the PET domain in the blend polymer and the neat PET. The sample was heated from 40 to 280°C at a rate of 10°C min^{-1}. The crystallinity was calculated using 140 J g^{-1} as the heat of fusion of 100% crystalline PET. [32]

With the exception of samples used to measure T_g and the interfacial tension, all samples were CO_2-annealed at 60°C and 10 MPa for 22.3 h so that the condition of the samples was analogous to that prior to foaming.

Characterization of blend and foam morphology

Scanning electron microscopy (SEM) was used to observe the blend and cell morphology of the foam. The samples were frozen in liquid nitrogen to create cryogenic fractural surfaces and then coated with gold for 180 s before observation under a SEM (Tiny-SEM 1540, Technex Co. Ltd., Japan) or field emission SEM (JSM-6700F, Jeol, Japan). FESEM images were collected at an acceleration voltage of 10 kV, a current of 5 μA, and a wide distance of 8 mm. The image processing software Image-J was used to

calculate the dispersed domain density, N_d, and the number average domain radius, $\overline{R_d}$, from the SEM micrographs.

$$\overline{R_d} = \frac{1}{c}\sum_{i}^{c} R_i \tag{1}$$

$$N_d = \frac{\phi}{\overline{V_c}} = \frac{\phi}{\frac{4}{3c}\pi\sum_{i}^{c} R_i^3} \tag{2}$$

where R_i is the radius of the i-th domain measured from the SEM micrographs. $\overline{R_d}$ is the average domain radius. ϕ is the volume fraction of the dispersed domain, and it is calculated from the weight ratios and densities of both polymers.

The interfacial area between the dispersed domain and the matrix per unit volume of blend, S, is calculated by:

$$S = N_d \overline{S_d} = N_d \frac{4}{c}\pi\sum_{i}^{c} R_i^2 \tag{3}$$

where $\overline{S_d}$ is the number average domain surface.

The cell density with respect to the solid polymer, N_f, and the number average cell radius, $\overline{R_n}$, were also calculated from the SEM micrographs. The bulk densities of the samples before and after foaming were measured by a densitometer (Mirage Electronic Densimeter MD-200S) and were used to calculate the cell density. The cell density with respect to the solid polymer was then calculated by the following: [33]

$$N_f = \frac{\rho_s}{\rho_f}\left(\frac{n}{A}\right)^{1.5} \tag{4}$$

where n is the number of bubbles in a total area, A. ρ_f and ρ_s are the densities of the foam and the solid bulk, respectively. Here, ρ_s / ρ_f is also known as the foam expansion ratio.

A gas pycnometer (AccuPyc, Shimadzu Corp.) was used to measure the volume of samples. The volume (V_{mea}), excluding the open pores, was measured by the gas pycnometer. The apparent volume of the samples (V_{app}) was measured geometrically using a caliper. Thus, the open-cell content (ε) and open-cell ratio (ε_r) were then calculated by the following: [11]

$$\varepsilon = \frac{V_{app} - V_{mea}}{V_{app}} \tag{5}$$

$$\varepsilon_r = \frac{\varepsilon}{1 - \rho_f / \rho_s} \tag{6}$$

The open-cell content (ε) indicates the volume fraction of open cells in the foam, and the open-cell ratio (ε_r) indicates the volume ratio of open cells to total (open + closed) cells.

The thickness of the cell wall (δ) was calculated by the following: [2]

$$\delta = d\left(\frac{1}{\sqrt{1 - \rho_f / \rho_s}} - 1\right) \tag{7}$$

where d is the average cell diameter.

THEORY OF BLEND CHARACTERIZATION IN BRIEF

Component fraction from the Fox equation

The T_g of a miscible polymer blend can be estimated by the Fox equation. When the equation is applied to partially miscible polymer blends, the minor polymer is commonly assumed to homogeneously infuse the major polymer phase. With this

assumption, we applied the Fox equation to the PET/PC blends to estimate the weight fraction of PET in the PC matrix and that of PC in PET. [34, 35]

$$\frac{1}{T_g^{'}} = \frac{\omega_{PET}^{'}}{T_{gPET}} + \frac{\omega_{PC}^{'}}{T_{gPC}} \tag{8}$$

and

$$\frac{1}{T_g^{''}} = \frac{\omega_{PET}^{''}}{T_{gPET}} + \frac{\omega_{PC}^{''}}{T_{gPC}} \tag{9}$$

where $\omega_{PC}^{'}$ is the weight fraction of PC infused in the PET domain and $\omega_{PET}^{'}$ (:=1-$\omega_{PC}^{'}$) is the weight fraction of PET in the PET domain. $\omega_{PET}^{''}$ (:=1-$\omega_{PC}^{''}$) is the weight fraction of PET in the PC matrix, and $\omega_{PC}^{''}$ is the PC weight fraction in the PC matrix. $T_g^{'}$ and $T_g^{''}$ are the glass transition temperatures of the PET domain and the PC matrix, respectively. T_{gPET} and T_{gPC} are the glass transition temperatures of the neat PET and the neat PC, respectively.

The weight fractions of PC in the PET domain and of PET in the PC matrix were calculated using Eqs. (10) and (11) with the T_g data of the blend and the neat polymers.

$$\omega_{PC}^{'} = \frac{T_{gPC}(T_{gPET} - T_g^{'})}{T_g^{'}(T_{gPET} - T_{gPC})} \qquad =1-\omega_{PET}^{'} \tag{10}$$

and

$$\omega_{PET}^{''} = \frac{T_{gPET}(T_{gPC} - T_g^{''})}{T_g^{''}(T_{gPC} - T_{gPET})} \qquad =1-\omega_{PC}^{''} \tag{11}$$

Furthermore, the weight fractions of both the PET domain and the PC matrix could be calculated from mass balance equations, which can be derived by transforming Eqs. (10)-(11).

$$\omega^{'} = \frac{\omega_{PC} - \omega_{PC}^{''}}{\omega_{PC}^{'} - \omega_{PC}^{''}} \tag{12}$$

and

$$\omega^{''} = \frac{\omega_{PC} - \omega_{PC}^{'}}{\omega_{PC}^{''} - \omega_{PC}^{'}} \tag{13}$$

where $\omega^{'}$ is the estimate of the weight fraction of the PET domain, $\omega^{''}$ is the estimate of the weight fraction of the PC matrix in the blend after transesterification reaction and ω_{PC} is the weight fraction (70% or 90%) of the PC matrix in the blend before transesterification reaction. [34, 35]

Estimate of interfacial tension

The storage modulus for the relaxation process, i.e., G' at the secondary plateau, is directly related to the interfacial tension between the dispersed domain and the matrix polymer. [36] The Palierne model was used to calculate the interfacial tension between two polymers. The model relates the dynamic modulus of emulsions with the dynamic modulus of the two phases, the size of the droplets, and the interfacial tension. [37]

$$G^{*} = G_m^{*}\left[\frac{1 + 3/2\sum_i \frac{\phi_i E_i}{D_i}}{1 - \sum_i \frac{\phi_i E_i}{D_i}}\right] \tag{14}$$

$$E_i = 2(G_d^{*} - G_m^{*})(19G_d^{*} + 16G_m^{*}) + \frac{48\beta_d^{*}\Gamma^0}{R_i^2} + \frac{32\beta_s^{*}(\Gamma^0 + \beta_d^{*})}{R_i^2} + \frac{8\Gamma^0}{R_i}(5G_d^{*} + 2G_m^{*}) + \frac{2\beta_d^{*}}{R_i}(23G_d^{*} - 16G_m^{*}) + \frac{4\beta_s^{*}}{R_i}(13G_d^{*} + 8G_m^{*}) \tag{15}$$

and

$$D_i = (2G_d^* + 3G_m^*)(19G_d^* + 16G_m^*) + \frac{48\beta_d^*\Gamma^0}{R_i^2} + \frac{32\beta_s^*(\Gamma^0 + \beta_d^*)}{R_i^2} + \frac{40\Gamma^0}{R_i}(G_d^* + G_m^*) + \frac{2\beta_d^*}{R_i}(23G_d^* + 32G_m^*) + \frac{4\beta_s^*}{R_i}(13G_d^* + 12G_m^*) \quad (16)$$

where Γ^0 is the interfacial tension. G_d^*, G_m^*, and G^* are the complex moduli of the dispersed domain, matrix, and emulsion (immiscible polymer blend), respectively, over a range of frequencies. ϕ_i is the volume fraction of a domain with radius R_i. β_d^* is the surface dilatation modulus associated with the domain dispersion, and β_s^* is the surface shear modulus attributed to the resistance of the interface to shear deformation. Both complex moduli depend on the frequency.

β_d^* is usually associated with the non-uniformity of the interface, and β_s^* is associated with the resistance to shear deformation. We assumed that the interface is uniformly composed of the copolymer such that the surface dilatation modulus, β_d^*, can be ignored. However, due to the shear deformation resistance of the copolymer, β_s^* should be expressed by the following: [37]

$$\beta_s^* = \beta_s^{'} + \beta_s^{''} \quad (17)$$

for $\omega\lambda_\beta < 1$:

$$\beta_s^{'} = \beta_0 \quad (18)$$

$$\beta_s^{''} = \beta_0\omega\lambda_\beta \quad (19)$$

for $\omega\lambda_\beta > 1$:

$$\beta_s^{'} = \beta_s^{''} = \beta_0\sqrt{\omega\lambda_\beta} \quad (20)$$

where β_0 is a low-frequency plateau in the storage modulus for the copolymer and λ_β is a characteristic relaxation time.

ϕ_i and R_i were measured from the SEM micrographs of the blend morphology. G_d^* and G_m^* were determined by individually measuring the complex moduli of the domain and matrix polymers. Γ^0 and β_0 were then determined by fitting the model estimates of the complex moduli to the experimental data. The detailed procedure for calculating the interfacial tension can be found elsewhere. [37]

RESULTS AND DISCUSSION

Characterization of blend properties

Figure 1 shows the shear loss moduli (G'') of the PET/PC blends with a 30/70 blend ratio. The T_g of the polymer was determined by the temperature at which the G''-temperature curve reached a peak. [38] The measured T_g of the neat PET and PC were 70.4°C and 147.7°C, respectively. The T_g of the PET-dispersed domains in the blend, denoted $T_g^{'}$, increased from that of neat PET to 79.1°C. The T_g of the PC matrix, $T_g^{''}$, decreased from that of neat PC to 124.4°C by mixing and heat annealing. The miscibility between PET and PC was increased at the interface by the presence of the PET-b-PC copolymer. Therefore, the two T_g values approached one another. The copolymer was produced by a transesterification reaction and was characterized by nuclear magnetic resonance (NMR) and Fourier transform infrared spectroscopy (FTIR). [26] The Fox equation was applied by assuming that the PET segment of the copolymer infuses and uniformly disperses into the PC matrix and that the PC segment also infuses into the PET

domain. This equation was then used to estimate the weight fraction of PET that infused the PC matrix and the weight fraction of PC that infused the dispersed PET domains. The calculated weight fractions are listed in Table 2. The details of the calculations are given elsewhere. [35, 39] By conducting the transesterification reaction at 280°C, the degrees of PET segment infusion into the PC matrix and of PC infusion into the PET-dispersed domains both increased. The weight fractions of the PET domains and PC matrix were obtained from Eqs. (12) and (13) and used to calculate the crystallinity of the PET domains, domain density, and interfacial area between the PET domains and the PC matrix.

Figure 2 shows the SEM micrographs of the PET/PC blend with a 30/70 blend ratio. A sea-island morphology was observed in most of the blends. The dispersed domains consisted of PET, whereas the matrix consisted of PC. The domain size decreased as the heat-annealing time increased for the blend with a 30/70 PET/PC blend ratio. The rheological data of the blends indicates that a longer heat-annealing time could produce more copolymer and increase the miscibility between the PET domains and the PC matrix. Consequently, the diameter of the domains decreased.

The domain size was measured and used to calculate the interfacial tension. The values of the interfacial tension are given in Table 3. The interfacial tension was determined by fitting the Palierne model to the experimental data of the storage and loss moduli. Figure 3 shows the experimental data and the model estimates for the PET/PC blends with a 30/70 blend ratio. The validity of the Palierne model was confirmed in our previous study on Poly(methyl methacrylate) (PMMA)/PC and PMMA/PP blends. [25] The model also agreed well with the experimental data for the PET/PC blends. The non-

heat-annealed PET/PC blend, A0, exhibited the largest interfacial tension, 2.3 mN m^{-1}, and blends A5 and B5 showed the smallest interfacial tensions, less than 0.01 mN m^{-1}. The interfacial tension inversely correlated with the heat-annealing time in both the 30/70 and 10/90 blends.

The domain diameter, $2\times\overline{R_d}$, the domain density, N_d, and the interfacial area per unit blend volume, S, were measured from SEM micrographs and calculated using Eqs. (1)-(3). The calculated values were plotted as a function of the interfacial tension, as shown in Figure 4. For PET/PC with a blend ratio of 30/70 (i.e., the A series), the size of the PET dispersed domains decreased from approximately 1.2 μm to 400 nm, the domain density and the interfacial area per unit volume of polymer blend increased as a result of the decreasing interfacial tension. In other words, the compatibility, uniformity and dispersion of the PET domains in the blend were drastically improved by increasing the copolymer, i.e., increasing the heat-annealing time. In contrast, the PET domain size was 300 nm without heat annealing for PET/PC with a blend ratio of 10/90 (i.e., B0), and it did not change with the decrease in interfacial tension, as shown in Figure 4-a. Furthermore, the domain density and the interfacial area per unit volume of the polymer blend showed results opposite to those of the PET/PC blend with a 30/70 blend ratio (Figure 4-b and c): the domain density and interfacial area both decreased when the interfacial tension decreased. Because of the low volume fraction of PET in the 10/90 wt% PET/PC blends (Table 2), the PET domains could be well dispersed without heat annealing. The amount of copolymer correlated positively with the heat annealing time. However, increasing the amount of copolymer enhanced the infusion of PET segments into the PC matrix rather than improving the PET domain dispersion and uniformity in

the blend. As the heat-annealing time increased and the interfacial tension decreased, the small PET domains tended to disappear because PET was transformed into the copolymer, which was infused into the PC matrix. Therefore, both the PET domain density and the interfacial area per unit volume of the blend polymer decreased in the 10/90 wt% PET/PC blends as the interfacial tension decreased.

Figure 5 shows the DSC curves of the neat PET and PET/PC blends with a 30/70 wt% blend ratio annealed under 10 MPa-CO_2 at 60°C for 22.3 h. The thermal properties measured by DSC are summarized in Table 4. The PET crystallized even though the CO_2-annealing temperature for A0, A1, and A5 was lower than the glass transition temperatures of the neat PET and the PET phase in the blends. This crystallization can be attributed to the plasticization effect of CO_2. Two peaks were detected in both the neat PET and blends (A0, A1). When the neat PET and its blends were CO_2-annealed, a secondary crystallization occurred, which was detected by the peak of the heat curve at approximately 110°C. The peaks of the secondary and primary crystals were, respectively denoted T_{m2} and T_{m3} in Figure 5. As shown in Table 4, the enthalpy of fusion of the primary crystals, ΔH_3, decreased as the amount of copolymer increased; T_{m2} could not be clearly detected in blends A5 because it overlapped with the glass transition temperature of PC: the melting point of the secondary crystals, T_{m2}, increased while that of the primary crystals, T_{m3}, decreased as the amount of copolymer increased. This relationship indicates that the crystalline structures of the primary crystals thinned and became less perfect while those of the secondary crystals thickened as the amount of copolymer increased. The melting points of the primary and secondary crystals often move in opposite directions. [40]

The crystallization of the polymers is also affected by the size of the dispersed domain. [41] Tol et al. reported a homogeneous nucleation process for a Polystyrene (PS)/Styrene-maleic anhydride (SMA)/Polyamide (PA6) blend in submicron dispersed PA6 domains. The imperfect crystals had a very low melting temperature compared with the primary and secondary crystals. In samples A5, B0, B1 and B5, the dispersed PET domain size was less than 500 nm (Figure 4-a). Therefore, the nucleation induced in the PET domains tended to be homogeneous because the size was too small for crystals to exist. The corresponding peak was then denoted T_{m1}, as shown in the enlarged section in Figure 5. The total crystallinity was calculated from the enthalpy of the primary crystals (ΔH_3), the enthalpy of the secondary crystals (ΔH_2) and the enthalpy of the crystals induced by the homogeneous nucleation in the submicron dispersed PET domains (ΔH_1). The total crystallinity decreased from 29% to 7.8% in the 30/70 blend ratio PET/PC and from 26% to 9.4% in the 10/90 blend ratio PET/PC.

The master curves of the PC and PET/PC blends with a 30/70 wt% blend ratio are shown in Figure 6. The viscoelastic modulus of all samples originated in the glassy zone ($G'>10^8$ Pa), moved from the transition zone to the plateau zone (10^7 Pa$>G'>10^6$ Pa) and finally reached the terminal zone ($G'<10^5$ Pa). When the samples were foamed at either 80, 120 and 150°C, they were mostly in the rubbery state, in which the polymer chains could move to create voids and the elasticity of the polymer matrix could still maintain its shape. As shown in Figure 6, the elasticity of PC was higher than that of the PET/PC blends over the entire frequency range. As the heat-annealing time increased, the amount of the PET segments that infused the PC matrix increased and the elasticity of the

PET/PC blends decreased. Furthermore, the T_g of PC decreased, along with the elasticity and viscosity of the PC matrix.

Figure 7 shows the uniaxial extensional viscosity of the PC and the PET/PC blends (A0, A1, and A5). The viscosity measurements were conducted at four different constant strain rates, 0.1, 0.2, 0.5, and 1.0 s^{-1}, at 240°C for all samples, except for blend A5. Blend A5 was measured at 220°C to prevent it from sagging during the measurement. None of the samples showed any strain hardening behavior.

Cell morphology of foamed blends

After dissolving CO_2 into the samples at 10 MPa and 60°C for 22.3 h, the samples were foamed at three different temperatures, 80, 120, and 150°C. Under these foaming conditions, bubble nucleation occurred only in PC and not in the PET domain due to the presence of crystals. However, the PET domains could serve as the bubble nucleating agents. Figures 8 and 9 show the SEM micrographs of the foamed PET/PC blends (A0-A5) and (B0-B5), respectively. The higher magnification SEM micrographs are also shown in Figures 10 and 11. All foams showed a spherical cell geometry. As the foaming temperature increased, the cells impinged on each other and the cell wall thickness was reduced. The higher magnification SEM images in Figures 10 and 11 show that the foam of blend A0, which had the largest interfacial tension, showed smooth cell walls. The PET domain seems to function as a bubble nucleating agent, and bubble nucleation occurred at the weak interface between the PET and PC. The foams of blend A1 and B0, which had the reduced interfacial tension and PET crystallinity, showed a fibril-like structure around the PET domains. The lowered interfacial tension and the infusion of copolymer into PET and PC increased the bonding force between PET and PC. The

bonding force then stretched the crystal lamellas in the PET domains to form the fibril-like structure. Further increasing the heat-annealing further decreased the interfacial tension. Moreover, the crystallinity of the PET domains also decreased. Therefore, the degree of fibrillation decreased, as shown in the micrograph of foamed blends A5, B1, and B5. Therefore, blends A1 and B0 showed a higher degree of fibrillation than blends A5, B1, and B5, in which the PET domains had a much lower crystallinity. These findings indicated that the fibril-like structure was generated by stretching the crystalline lamellas in the PET domains in the presence of bonding forces between PET and PC.

The cell density and the cell size were measured from the SEM micrograph, and the results are illustrated in Figure 12. The cell density of blends A0, A5, B1, and B5 decreased as the foaming temperature increased, as shown in Figure 12. Only blends A1 and B0, which showed a highly fibrillar cell morphology, showed an increase in the cell density as the foaming temperature increased. A higher foaming temperature led to a larger degree of supersaturation and increased the cell density per unit volume of the solid polymer. The decreased cell density for blends A0, A5, B1, and B5 could be attributed to cell coalescence that resulted from a decrease in the viscosity at high foaming temperatures. The increase in the cell density for blends A1 and B0 was not induced by the suppression of cell coalescence because neither blend showed strain hardening behavior. However, this increase could be related to the formation of fibril-like structures. The bubble nucleation mechanism in blends A1 and B0 could likely differ from that of blends A0, A5, B1, and B5. This difference might be related to the stretch-induced void formation in crystalline polymers.

The open-cell content (volume fraction of open cells in the polymeric foam) of all foamed samples was measured. The open-cell ratio (volume ratio of open cells to total cells) and cell wall thickness were then calculated using Eqs. (6) and (7). The results are presented in Figures 13 and 14. Increasing the foaming temperature increased the expansion ratio. This increase, in turn, increased the open-cell content of most of the foams. Nevertheless, blends A1 and A5 shrank when they were foamed at 150°C because the foaming temperature was much higher than the glass transition temperature of the matrix polymer PC. Thus, their expansion ratio was not increased with the increase in the foaming temperature, which also prevented the open-cell content from increasing. Figure 14 also shows that the open-cell ratio increased monotonously as the cell walls thinned. The PET/PC 10/90 wt% blend performed better overall with respect to the cell density, cell size and open-cell content. The fibril-structure of blend B0 could provide the high open-cell content with the low expansion ratio.

CONCLUSIONS

In this study, we reported a novel method for controlling the foam morphology of open-cell foams by forming fibril-like structures around the PET domains. Heat annealing was a critical process for modifying the interfacial properties by forming a copolymer at the interface between the PET and PC phases. The interfacial tension decreased, the affinity between PET and PC increased, and the crystallinity of the PET domains decreased as the amount of copolymer increased. When the interfacial affinity was strong, a fibril-like structure formed during CO_2 foaming by stretching the crystalline lamellas in the PET domains. The degree of fibrillation was a function of the crystallinity

of the PET domains. When the heat-annealing procedure was optimized to generate a large degree of fibrillation during CO_2 foaming, PET/PC blend foams with a large cell density (7×10^{11} # cm^{-3}), a small cell size (less than 2 μm), and 100% open cells were generated.

REFERENCES

1. H. Ruckdaschel, P. Gutmann, V. Altstadt, H. Schmalz, A.H.E. Muller, *Adv. Polym. Sci.*, **227**, 199 (2010).

2. D. Klempner, K.C. Frisch, *Handbook of Polymeric Foams and Foam Technology*, New York (1991).

3. M. Mantovani, C. Gastagnetti, P.P. Godano, H. Yamaguchi, Japan Patent, 4279,624 (2005).

4. D.T. Wong, S.A. Mullin, V.S. Battaglia, N.P. Balsara, *J. Membr. Sci.*, **394-395**, 175 (2012).

5. X. Liao, H. Zhang, T. He, *J. Nanomater*., 1 (2012).

6. P.C. Lee, G. Li, J.W.S. Lee, C.B. Park, *J. Cell. Plast.*, **43**, 431 (2007).

7. P.C. Lee, H.E. Naguib, C.B. Park, J. Wang, *Polym. Eng. Sci.*, **45**, 1445 (2005).

8. D. Kohlhoff, M. Ohshima, *Macromol. Mater. Eng.*, **296**, 770 (2011).

9. P.C. Lee, J. Wang, C.B. Park, *Ind. Eng. Chem. Res.*, **45**, 175 (2006).

10. C.B. Park, V. Padareva, P.C. Lee, H.E. Naguib, *J. Polym. Eng.*, **25**, 239 (2005).

11. R. Miyamoto, M. Fukumori, H. Shikuma, M. Ohshima, *Proceeding of the Polymer Processing Society 28th Annual Meeting (PPS-28)*, Pattaya in Thailand (2012).

12. B. Krause, M.E. Boerrigter, N.F.A. van der Vegt, H. Strathmann, M. Wessling, *J. Membr. Sci.*, **187**, 181 (2001).

13. B. Krause, H.J.P. Sijbesma, P. Münüklü, N.F.A. van der Vegt, M. Wessling, *Macromolecules*, **34**, 8792 (2001).

14. B. Krause, K. Diekmann, N.F.A. van der Vegt, M. Wessling, *Macromolecules*, **35**, 1738 (2002).

15. Y. Li, Z. Yao, Z. Chen, K. Cao, S. Qiu, F. Zhu, C. Zeng, Z. Huang, *Chem. Eng. Sci.*, **66**, 3656 (2011).

16. W. Zhai, H. Wang, J. Yu, J. Dong, J. He, *Polym. Eng. Sci.*, **48**, 1312 (2008).

17. Q. Liao, A. Tsui, S. Billington, C.W. Frank, *Polym. Eng. Sci.*, **52**, 1495 (2012).

18. W. Zhai, J. Wang, N. Chen, H.E. Naguib, C.B. Park, *Polym. Eng. Sci.*, **52**, 2078 (2012).

19. C.A. Kumar, J. Krishnamurthy, *Polym. Eng. Sci.*, **51**, 1749 (2011).

20. P. Spitael, C.W. Macosko, *Polym. Eng. Sci.*, **44**, 2090 (2004).

21. P. Spitael, C.W. Macosko, R.B. McClurg, *Macromolecules*, **37**, 6874 (2004).

22. R.W. Sharudin, A. Nabil, K. Taki, M. Ohshima, *J. Appl. Polym. Sci.*, **119**, 1042 (2010).

23. W. Zhai, H. Wang, J. Yu, J. Dong, J. He, *J. Polym. Sci. Part B: Polym. Phys.*, **46**, 1641 (2008).

24. S. Siripurapu, J.M. DeSimone, S.A. Khan, R.J. Spontak, *Macromolecules*, **28**, 2271 (2005).

25. P. Gong, M. Ohshima, *J. Appl. Polym. Sci.*, Accepted.

26. P. Gong, M. Ohshima, *J. Polym. Sci. Part B: Polym. Phys.*, **50**, 1173 (2012).

27. T.R. Nassar, D.R. Paul, J.W. Barlow, *J. Appl. Polym. Sci.*, **23**, 85 (1979).

28. D. Ma, G. Zhang, Y. He, J. Ma, X. Luo, *J. Polym. Sci. Part B: Polym. Phys.*, **37**, 2960 (1999).

29. T. Suzuki, H. Tanaka, T. Nishi, *Polymer*, **30**, 1287 (1989).

30. Z. Zhang, Y. Xie, D. Ma, *Eur. Polym. J.*, **37**, 1961 (2001).

31. M. Fiorini, F. Pilati, C. Berti, M. Toselli, V. Ignatov, *Polymer*, **38**, 413 (1997).

32. P. Gong, T. Liu, L. Zhao, *J. Macromol. Sci. Part B: Phys.*, **50**, 329 (2011).

33. C.B. Park, P.C. Lee, J. Wang, V. Padareva, *Cell. Polym.*, **25**, 1 (2006).

34. R.S. Porter, L.H. Wang, *Polymer*, **33**, 2019 (1992).

35. N. Marin, B.D. Favis, *Polymer*, **43**, 4723 (2002).

36. D. Graebling, R. Muller, J.F. Palierne, *Macromolecules*, **26**, 320 (1993).

37. H. Asthana, K. Jayaraman, *Macromolecules*, **32**, 3412 (1999).

38. The Society of Polymer Science, *Kisokoubunnshikagaku*, Tokyo (2006).

39. W.N. Kim, C.M. Burns, *Macromolecules*, **20**, 1876 (1987).

40. Z.G. Wang, B.S. Hsiao, B.B. Sauer, W.G. Kampert, *Polymer*, **40**, 4615 (1999).

41. R.T. Tol, V.B.F. Mathot, G. Groeninckx, *Polymer*, **46**, 2955 (2005).

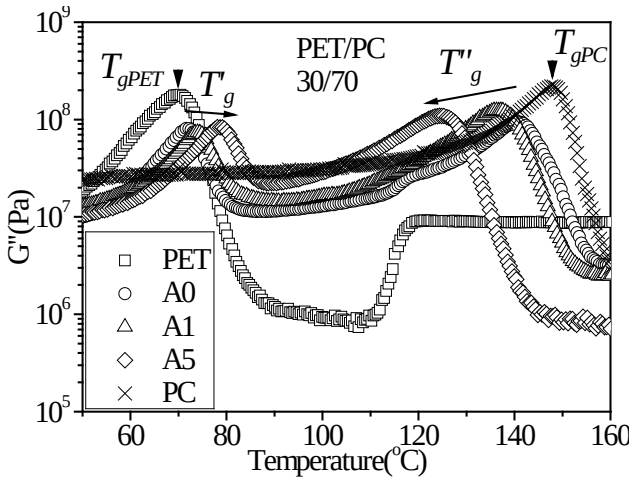

Figure 1 Shear loss moduli (G'') of PET, PC, and 30/70 wt% PET/PC blends (A0, A1, and A5)

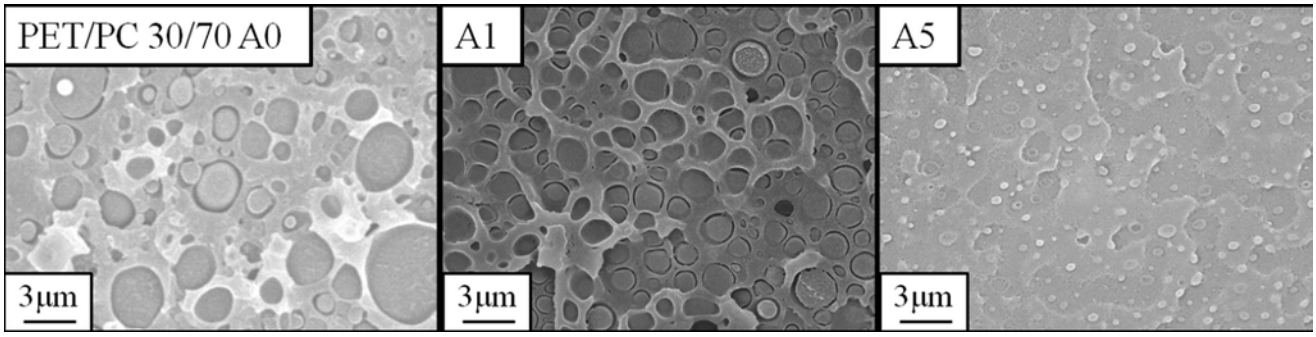

Figure 2 SEM morphology of the 30/70 wt% (A0, A1, and A5) PET/PC blends

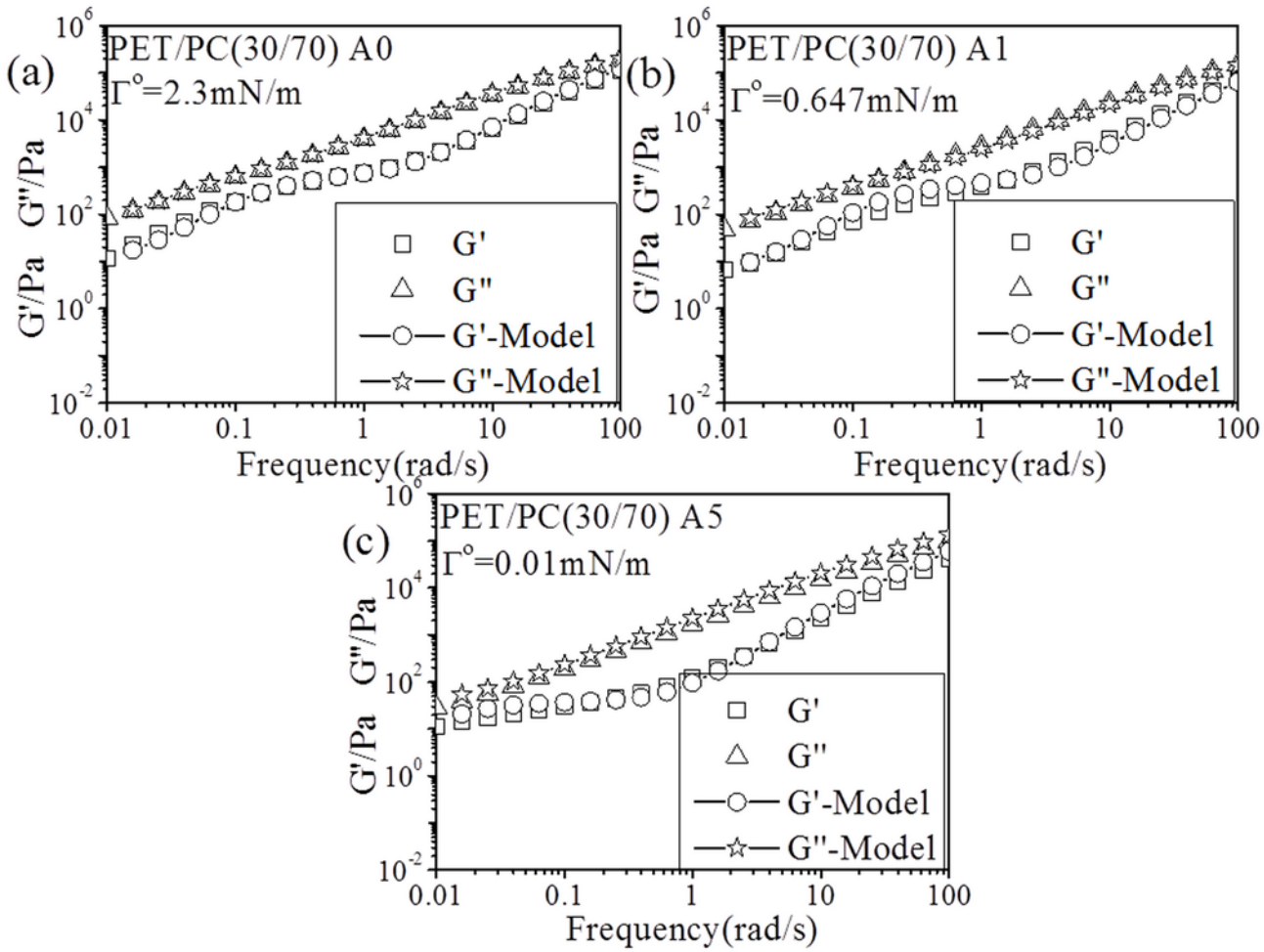

Figure 3 Estimates of the Palierne model and experimental data of the dynamic modulus

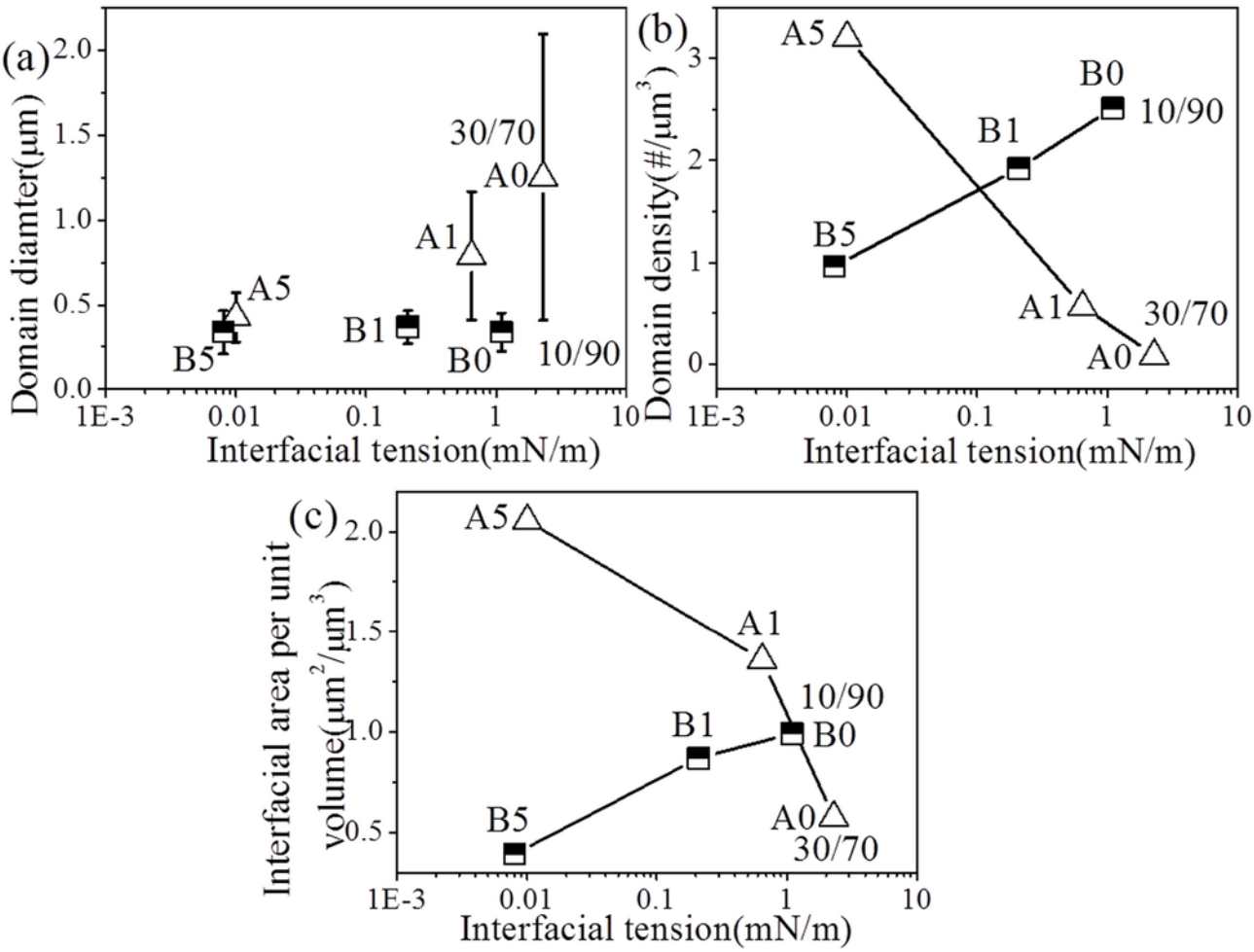

Figure 4 Number average domain diameter, $2\times\overline{R_d}$ (a), the dispersed domain density, N_d (b), and the interfacial area per unit blend volume, S (c) of the PET/PC blends

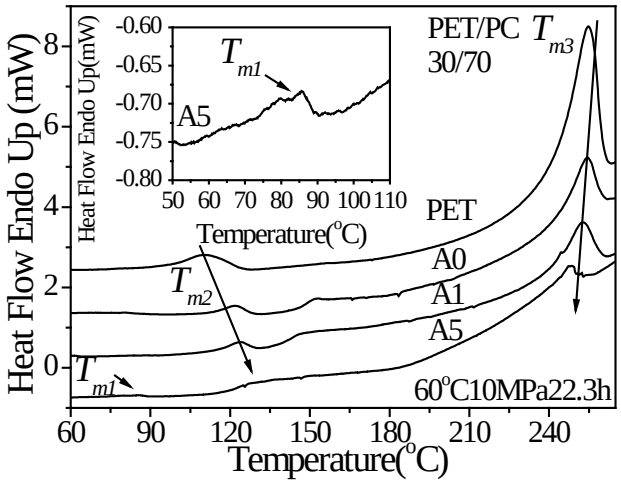

Figure 5 DSC heat curves of the neat PET and the PET/PC 30/70 wt% blends (A0, A1, and A5) after CO_2-annealing at 60°C 10 MPa for 22.3 h

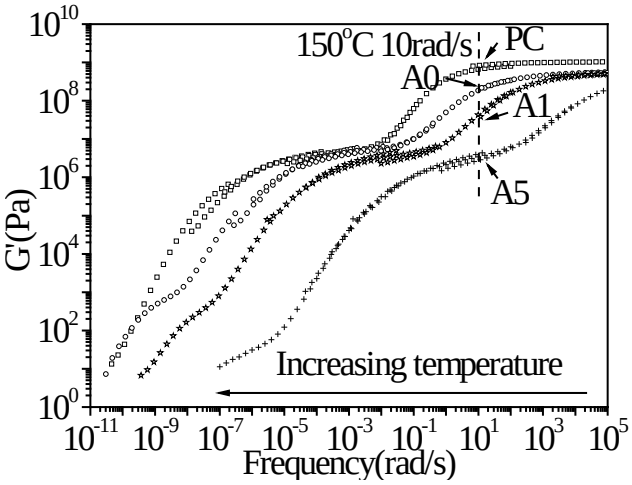

Figure 6 Master curves of the G' of PC and PET/PC 30/70 wt% blends (A0, A1, and A5) at 150°C

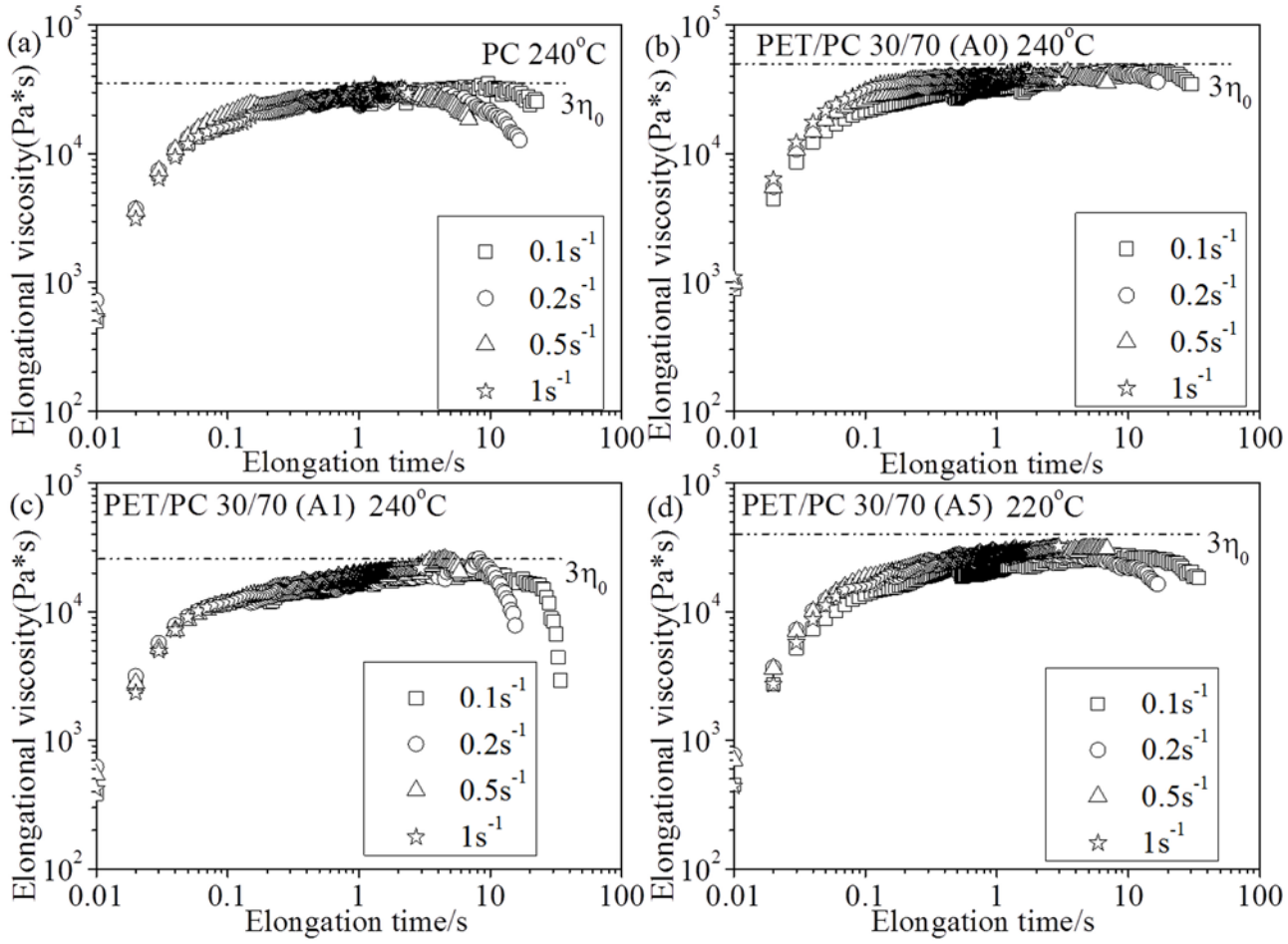

Figure 7 Uniaxial elongational viscosity of PC and PET/PC 30/70 wt% blends (A0, A1) at 240°C and the PET/PC 30/70 wt% blend (A5) at 220°C at different constant strain rates. Dashed lines represent the value of three times the zero shear viscosity

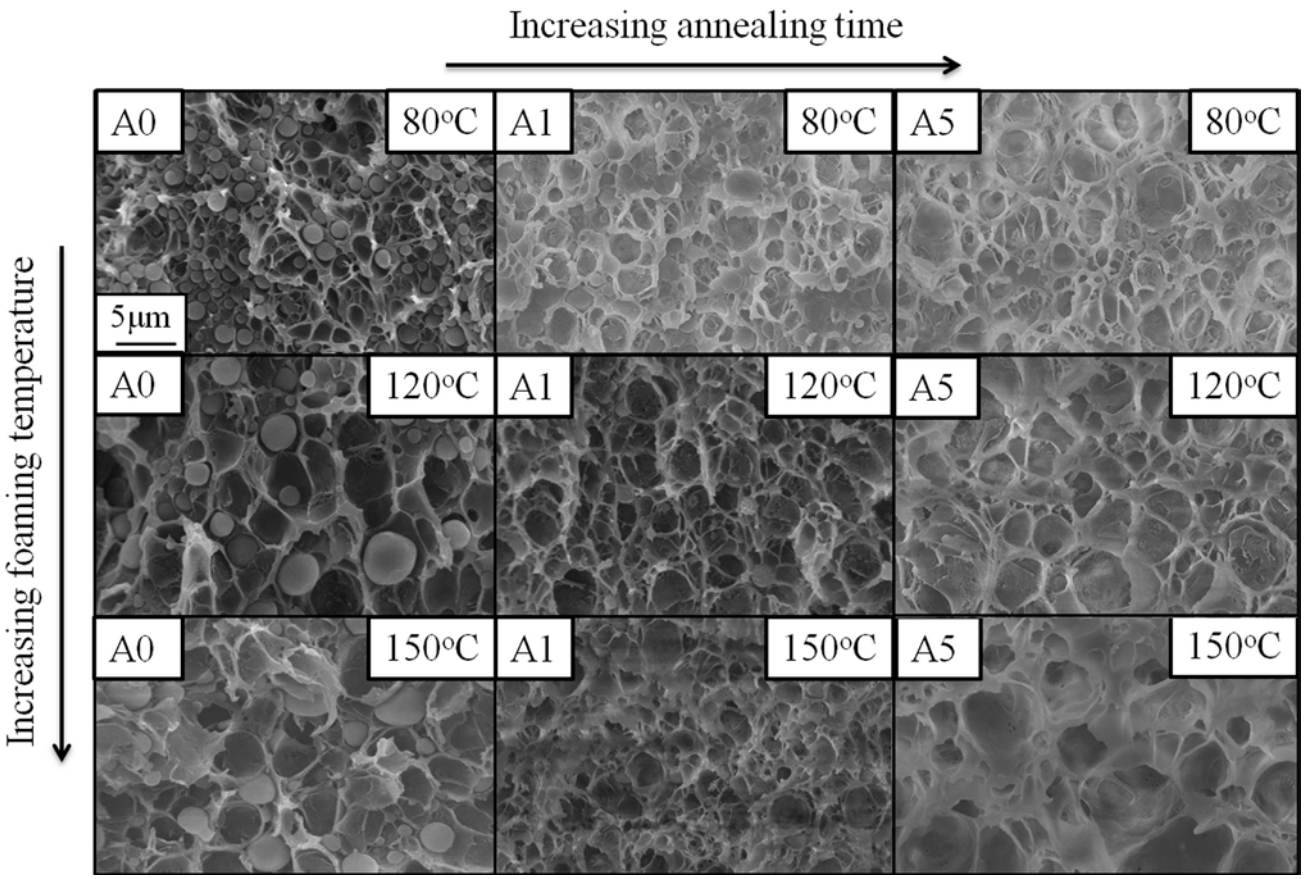

Figure 8 SEM micrographs of PET/PC 30/70 wt% blends (A0, A1, and A5) foamed at 80, 120, and 150°C (Magnification × 3000)

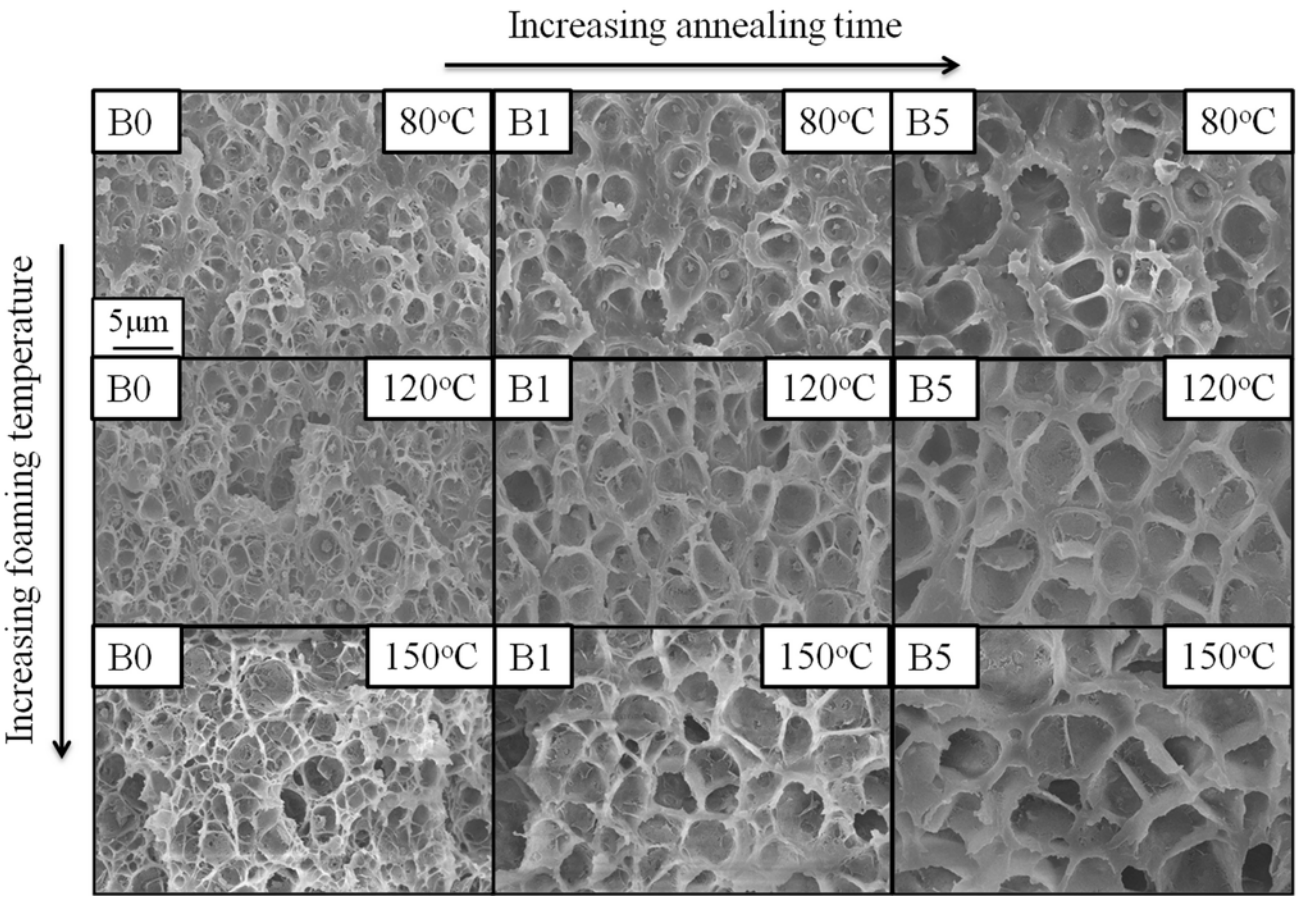

Figure 9 SEM micrographs of PET/PC 10/90 wt% blends (B0, B1, and B5) foamed at 80, 120, and 150°C (Magnification × 3000)

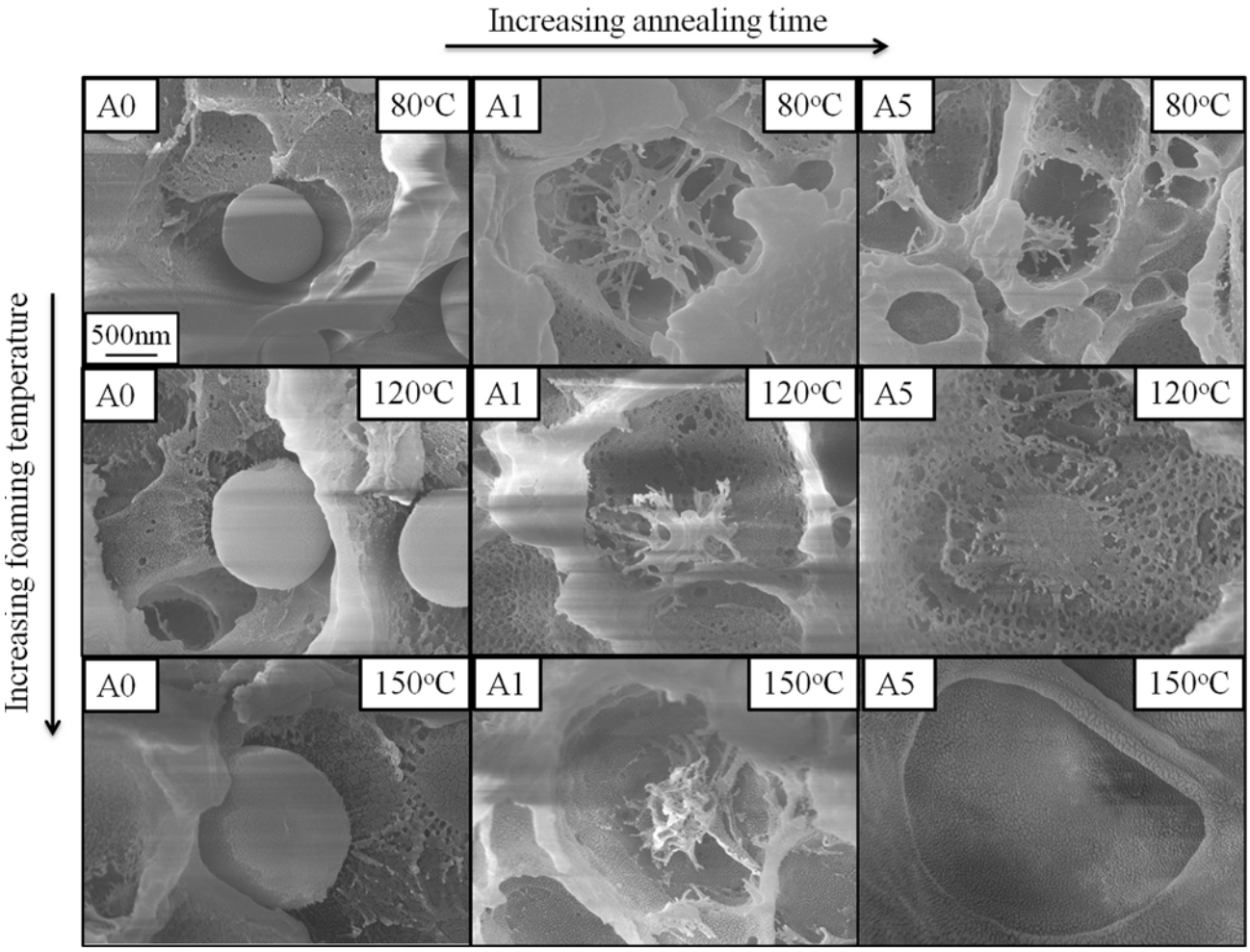

Figure 10 SEM micrographs of PET/PC 30/70 wt% blends (A0, A1, and A5) foamed at 80, 120, and 150°C (Magnification × 30000)

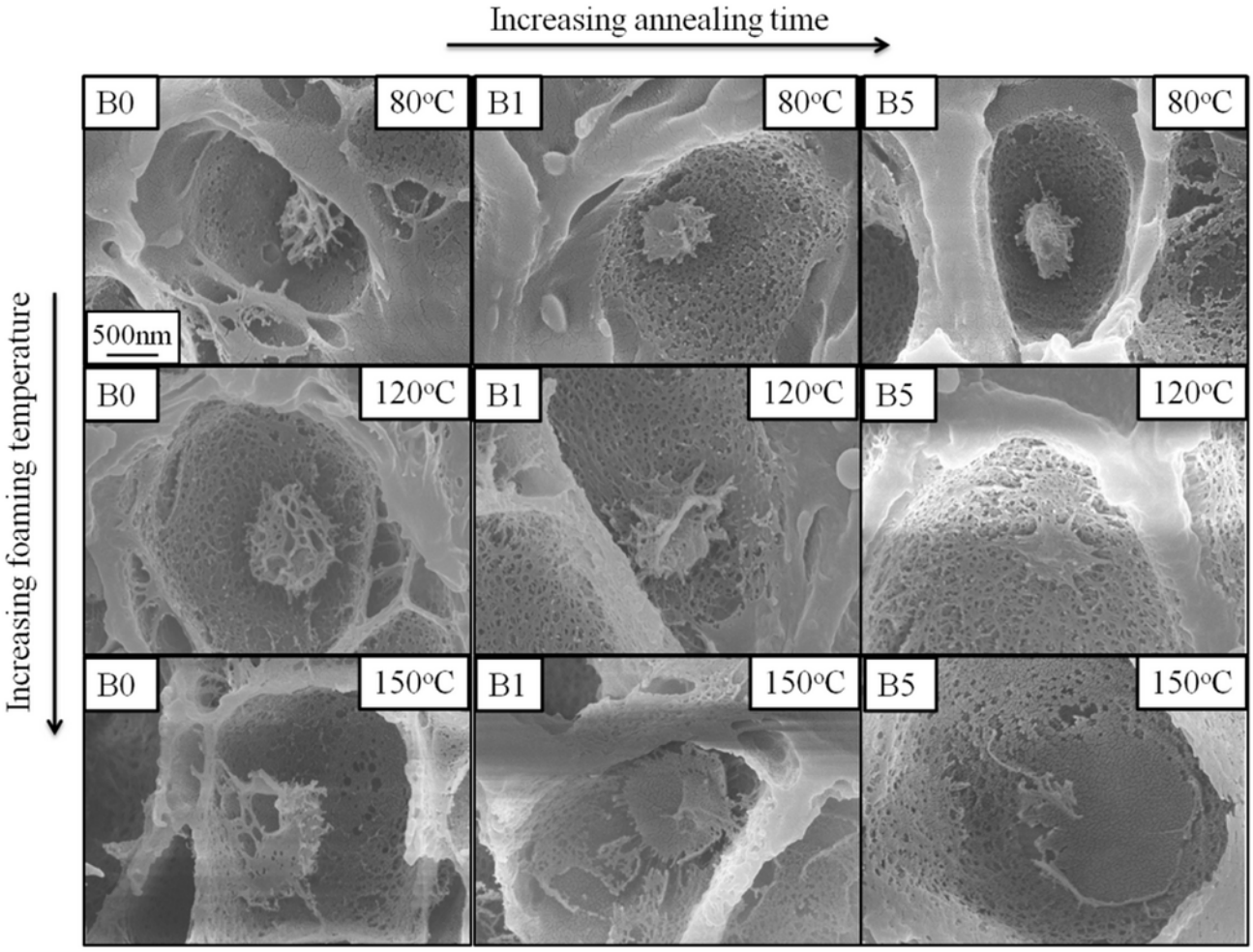

Figure 11 SEM micrographs of PET/PC 10/90 wt% blends (B0, B1, and B5) foamed at 80, 120, and 150°C (Magnification × 30000)

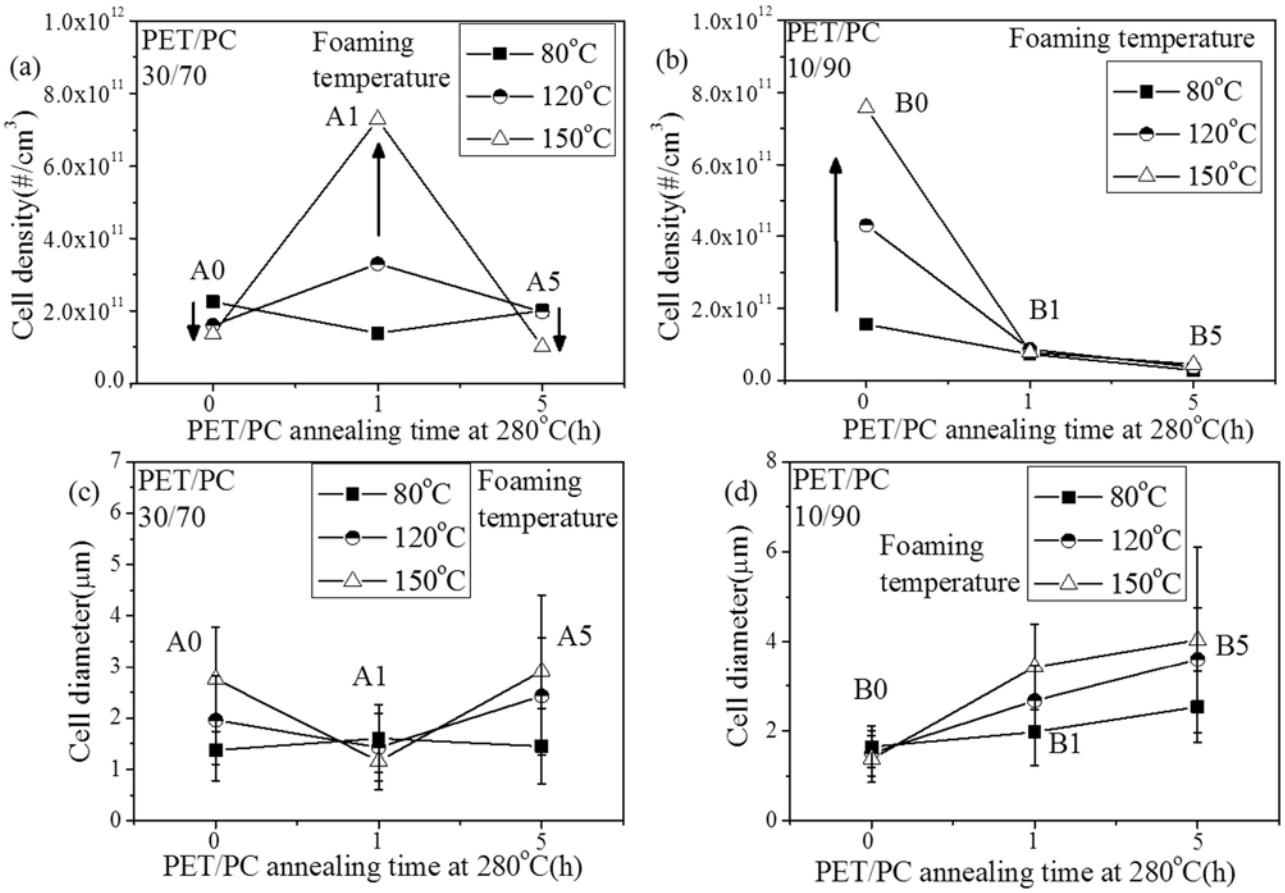

Figure 12 Cell density, (a) and (b), and cell size, (c) and (d), of the blends foamed at 80, 120, and 150°C

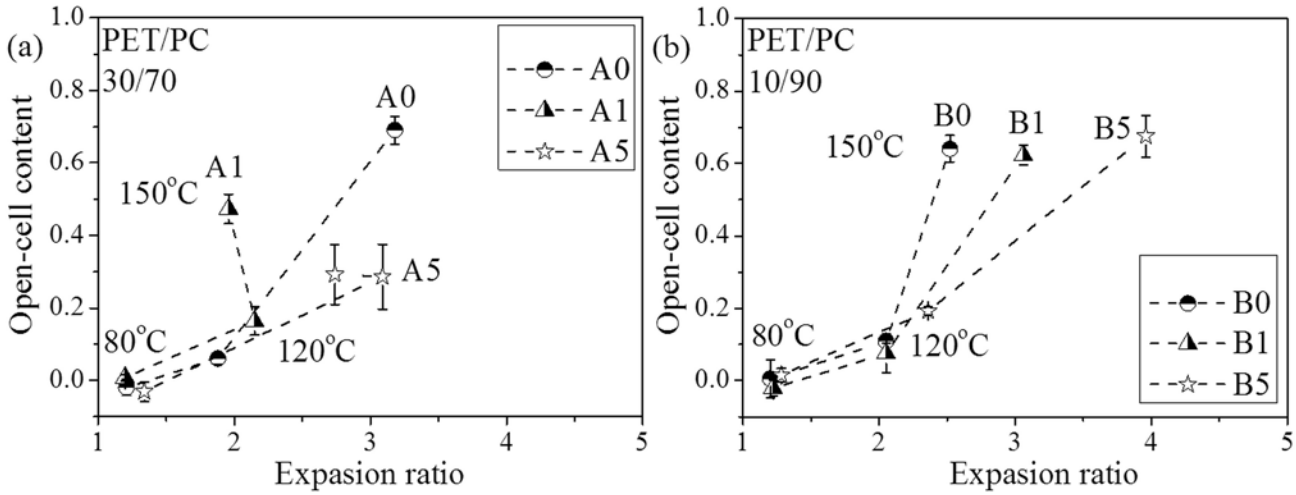

Figure 13 Open-cell content of PET/PC 30/70 wt% (a) and PET/PC 10/90 wt% (b) blends as a function of expansion ratio

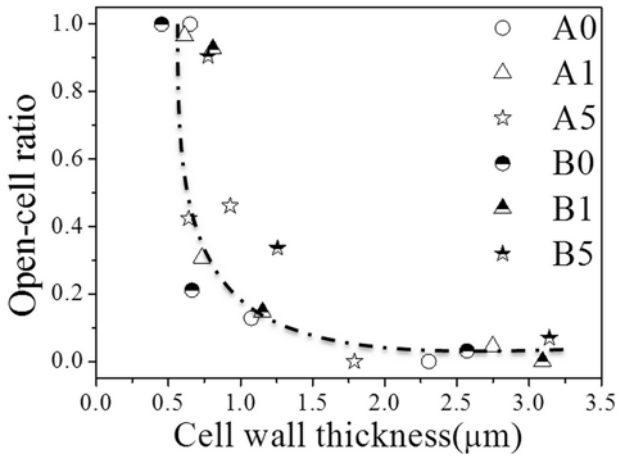

Figure 14 Open-cell ratio as a function of cell wall thickness

Table 1 Weight ratio, heat-annealing time, and sample ID. of PET/PC blends

Blend ratio	Heat-annealing time	Sample ID.
PET/PC 30/70	0 h	A0
	1 h	A1
	5 h	A5
PET/PC 10/90	0 h	B0
	1 h	B1
	5 h	B5

Table 2 T_g and the estimated weight percentages of PET and PC in the PET domain and PC matrix of the PET/PC blends

PET/PC		PET domain				PC matrix			
		$T_g^{'}$ (°C)	$\omega_{PET}^{'}$	$\omega_{PC}^{'}$	$\omega^{'}$	$T_g^{''}$ (°C)	$\omega_{PET}^{''}$	$\omega_{PC}^{''}$	$\omega^{''}$
30/70	**A0**	71.7	96.7%	3.3%	27.5%	140.5	4.6%	95.4%	72.5%
	A1	74.0	90.9%	9.1%	26.9%	136.3	7.6%	92.4%	73.1%
	A5	79.1	79.0%	21.0%	20.8%	124.4	17.1%	82.9%	79.2%
10/90	**B0**	72.5	94.6%	5.4%	8.0%	143.6	2.6%	97.4%	92.0%
	B1	73.9	91.1%	8.9%	7.1%	141.8	3.8%	96.2%	92.9%
	B5	75.9	86.2%	13.8%	3.3%	136.6	7.4%	92.6%	96.7%

Table 3 Interfacial tension calculated using the Palierne model

Blend component		Interfacial tension (mN/m)
PET/PC 30/70	**A0**	2.3
	A1	0.647
	A5	0.01
PET/PC 10/90	**B0**	1.1
	B1	0.21
	B5	0.008

Table 4 Thermal properties of the neat PET and PET/PC blends after CO_2-annealing at 60°C 10 MPa for 22.3 h

Sample ID.		T_{m1}(°C)	ΔH_1(J/g)	T_{m2}(°C)	ΔH_2(J/g)	T_{m3}(°C)	ΔH_3(J/g)	ΔH_{total}(J/g)	Crystallinity(%)
PET		-	-	112.5	4.07	254.7	46.1	50.2	36%
PET/PC	**A0**	-	-	122.6	1.11	254.9	10.2	11.3	29%
	A1	-	-	123.9	1.29	252.9	8.74	10.0	27%
30/70	**A5**	86.1	0.10	-	-	249.1	2.17	2.27	7.8%
PET/PC	**B0**	83.4	0.24	120.7	0.17	252.4	2.60	2.84	26%
	B1	84.6	0.16	120.6	0.13	242.4	0.73	1.02	10%
10/90	**B5**	-[a]	-[a]	-[a]	-[a]	241.8	0.44	0.44	9.4%

a – too small to be observed;